

# Hydrogen-Driven Cage Unzipping of $C_{60}$ into Nano-Graphenes

Alexandr V. Talyzin,<sup>\*†</sup> Serhiy Luzan,<sup>†</sup> Ilya V. Anoshkin,<sup>‡</sup> Albert G. Nasibulin,<sup>‡</sup> Esko I. Kauppinen,<sup>‡</sup> Andrzej Dzwilewski,<sup>§</sup> Ahmed Kreta,<sup>#</sup> Janko Jamnik,<sup>#</sup> Abdou Hassani,<sup>#</sup> Anna Lundstedt,<sup>⊥</sup> and Helena Grennberg<sup>⊥</sup>

<sup>†</sup>Department of Physics, Umeå University, SE-901 87 Umeå, Sweden

<sup>‡</sup>Department of Applied Physics, Aalto University, P.O. Box 15100, FI-00076 Aalto, Espoo, Finland

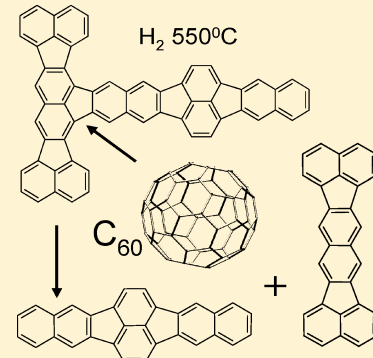
<sup>§</sup>Department of Physics and Electrical Engineering, Karlstad University, SE-651 88 Karlstad, Sweden

<sup>#</sup>National Institute of Chemistry, 19 Hajdrihova, Ljubljana 1000, Slovenia

<sup>⊥</sup>Department of Chemistry-BMC, Uppsala University, Box 576, SE-751 23 Uppsala, Sweden

## Supporting Information

**ABSTRACT:** Annealing of  $C_{60}$  in hydrogen at temperatures above the stability limit of C–H bonds in  $C_{60}H_x$  (500–550 °C) is found to result in direct collapse of the cage structure, evaporation of light hydrocarbons, and formation of solid mixture composed of larger hydrocarbons and few-layered graphene sheets. Only a minor part of this mixture is soluble; this was analyzed using matrix-assisted laser desorption/ionization MS, Fourier transform infrared (FTIR), and nuclear magnetic resonance spectroscopy and found to be a rather complex mixture of hydrocarbon molecules composed of at least tens of different compounds. The sequence of most abundant peaks observed in MS, which corresponds to  $C_2H_2$  mass difference, suggests a stepwise breakup of the fullerene cage into progressively smaller molecular fragments edge-terminated by hydrogen. A simple model of hydrogen-driven  $C_{60}$  unzipping is proposed to explain the observed sequence of fragmentation products. The insoluble part of the product mixture consists of large planar polycyclic aromatic hydrocarbons, as evidenced by FTIR and Raman spectroscopy, and some larger sheets composed of few-layered graphene, as observed by transmission electron microscopy. Hydrogen annealing of  $C_{60}$  thin films showed a thickness-dependent results with reaction products significantly different for the thinnest films compared to bulk powders. Hydrogen annealing of  $C_{60}$  films with the thickness below 10 nm was found to result in formation of nanosized islands with Raman spectra very similar to the spectra of coronene oligomers and conductivity typical for graphene.



## 1. INTRODUCTION

Fullerene  $C_{60}$  is a cage molecule formed by 20 carbon hexagons and 12 pentagons. The curvature of the molecule originates from pentagons, which make fullerenes more reactive compared to planar graphene, where the carbon atoms are bonded entirely in hexagons. For example,  $C_{60}$  easily reacts with molecular hydrogen at elevated conditions forming  $C_{60}H_x$  (also called fulleranes) with “ $x$ ” approaching the maximal possible value of 60,<sup>1–5</sup> while hydrogenation of graphene is more difficult and typically performed using atomic hydrogen.<sup>6</sup> Hydrogenation of fullerenes has been extensively studied over the past two decades as a route to possible high density hydrogen storage materials.<sup>4</sup> Recently published studies alkali metal doped  $C_{60}$  hydrogenation have revived the interest in this application of fulleranes.<sup>7,8</sup>

It is known that prolonged exposure of  $C_{60}$  to molecular hydrogen at 400–450 °C results first in formation of fulleranes  $C_{60}H_x$  ( $x$  up to 52), followed by cage fragmentation ( $C_{59}H_x$ ,  $C_{58}H_x$ , etc.) and collapse of cage structure with formation of a complex mixture of hydrocarbon molecules.<sup>9–15</sup> Large fullerene fragments, for example, polycyclic aromatic hydrocarbons (PAHs), have been identified as some of the final cage

fragmentation products. Formation of PAHs is expected under the conditions of hydrogenation reaction since any dangling bond that appears in the process of fullerene cage fragmentation will be immediately terminated by hydrogen.<sup>12,14</sup> The hydrogenation of the  $C_{60}$  cage is only partly reversible, especially for strongly hydrogenated samples.<sup>10</sup> Annealing of  $C_{60}H_x$  in inert gas or vacuum results in C–H bond breaking, hydrogen release, and at least partial recovering of pristine  $C_{60}$ . According to thermogravimetric analysis (TGA) experiments, the release of hydrogen occurs at around 480–550 °C.<sup>10,16–18</sup> Therefore, it can be expected that hydrogen reaction with  $C_{60}$  in this temperature region will proceed into direct breakup of the fullerene cage rather than formation of fulleranes.

Recently, we reported that increasing the temperature for the hydrogenation reaction above the limits of C–H bond stability in fulleranes induces rapid collapse of the  $C_{60}$  cage structure with formation of unidentified carbon/hydrogen products. The main aim of this previously published study was to observe

**Received:** January 13, 2014

**Revised:** February 27, 2014

**Published:** February 28, 2014



hydrogen-driven collapse of  $C_{60}$  inside carbon nanotubes.<sup>19</sup> Unexpectedly, we also found several single layered graphene sheets among “super-hydrogenated” peapods which could form only as a result of hydrogen reaction with carbon materials available in studied sample (fullerenes and carbon nanotubes). This intriguing observation motivated more detailed study of hydrogen-driven unzipping and collapse of  $C_{60}$  at around 550 °C.

Here, we report detailed study of hydrogen-driven unzipping of the  $C_{60}$  cage at elevated conditions (500–550 °C, 50 bar H<sub>2</sub> pressure) performed on both bulk powder and thin film samples. The reaction of  $C_{60}$  with hydrogen at higher temperatures leads to direct etching of the  $C_{60}$  cage. The fullerene molecule collapse induced by hydrogen is found to result in the formation of “nano-graphene” molecules, PAHs, and few-layered graphene sheets. Annealing  $C_{60}$  thin films in hydrogen at elevated conditions results in the formation of graphene islands with spectral characteristics similar to previously observed coronene oligomer samples.<sup>20,21</sup> On the basis of our results, we suggest a possible mechanism of the cage opening, fragmentation, and the formation of nanographenes.

## 2. EXPERIMENTAL SECTION

Fullerene  $C_{60}$  powder (>99.9%, MER Corporation, Tucson, Arizona, USA) was placed into an alumina container, sealed in a stainless steel reactor, and subjected to annealing in hydrogen at a pressure of about 50 bar and temperatures of 500–550 °C for 6–24 h. The weight of samples decreased as a result of the reaction of  $C_{60}$  with hydrogen due to evaporation of light hydrocarbons. Maximal weight loss of about 50% was observed for powder samples annealed under hydrogen at 550 °C for 24 h. Mass spectrometry was performed with a matrix-assisted laser desorption ionization time-of-flight (MALDI-TOF) mass spectrometer (Voyager DE-STR, Applied Biosystems, Carlsbad, California, USA). Nuclear magnetic resonance (NMR) spectra of the soluble fractions were recorded on a Varian UNITY (<sup>1</sup>H at 399.97 MHz, <sup>13</sup>C at 100.58 MHz) or a Varian INOVA (<sup>1</sup>H at 499.93 MHz, <sup>13</sup>C at 125.71 MHz) spectrometer. The chemical shift regions are reported using the residual solvent signal as an indirect reference to TMS (<sup>1</sup>H: CHCl<sub>3</sub>: 7.26, toluene-*d*<sub>8</sub>: 2.03 (CH<sub>3</sub>), <sup>13</sup>C: CDCl<sub>3</sub>: 77.0 ppm). Chemical shift simulations were performed using MestReNova v6.0.2 software (Mestrelab Research S.L. 2009). X-ray photoelectron spectra (XPS) were recorded with a Kratos Axis Ultra electron spectrometer equipped with a delay line detector. A monochromated Al KR source operated at 150 W, a hybrid lens system with a magnetic lens, providing an analysis area of 0.3 mm × 0.7 mm, and a charge neutralizer were used for the measurements. Raman spectra were recorded with 514 nm laser excitation using a Renishaw inVia Raman spectrometer. FT-IR spectra were collected using a Bruker IFS 66 v/S using transmission mode on finely ground KBr diluted samples. The high-resolution TEM images were collected on a JEOL JEM-2200FS with a corrector of spherical aberrations (Cs ≤ 0.005 mm). To minimize the destructive influence of electron irradiation, all samples were analyzed at 80 kV acceleration voltage and the minimal possible electron illumination time.

The C-AFM measurements (Veeco Multimode V, Veeco, USA/Nanonis, Specs, Switzerland) were carried out at room temperature in an ambient pressure environmental controlled chamber of 6.5 l in volume flushed with a flow of 99.99% of argon (Scientific Argon, Messer, Slovenia) at a constant flow

rate of 0.2 L/min. During measurement of IV curves, the doped diamond tip (Nanosensors DT-NCHR, Nanoworld AG, Switzerland) was brought into contact at a constant force of 0.2 nN. Resistances were estimated by performing current–voltage curve measurements at different points on the  $C_{60}$  transformed nanoislands. The islands resistances were estimated based on differential profile measurement over islands and gold substrate. The C-AFM tip cleanliness and contact reproducibility were checked on Au substrate before and after collecting data on islands to ensure good contact and linearity of the IV curves. The atomic force microscopy (AFM) imaging was carried out by conventional tapping mode, while electrical measurements were performed under constant force in AFM contact mode. Prior to contact, a slow approach soft landing was performed. This approach allows the tip to avoid jumping into contact, which has a high risk of damaging soft materials such as  $C_{60}$  nanoislands.<sup>22</sup> IV measurements were performed by ramping sample bias from −1 V to +1 V, while monitoring the current. The upper limit of the current was set to the μA range by connecting a limiting resistor of 1 M Ω in series with sample to protect it and the tip from electron migration.

The scanning tunneling microscopy (STM) topographic images were collected by recording the tip height at a constant sample bias. Typical imaging parameters are 2 V and 0.2 nA for bias voltage and tunneling current respectively.

## 3. RESULTS AND DISCUSSION

**3.1. Characterization of Carbon Deposits Formed from  $C_{60}$  Powder.** It was anticipated from our previous experience that hydrogen-driven  $C_{60}$  collapse results in complex mixtures of products that are difficult to analyze. The light hydrocarbons formed as a result of hydrogen treatment of  $C_{60}$  would evaporate from the samples leaving only relatively large hydrocarbons with melting points higher than the temperature of annealing. The residual material is particularly difficult for analysis as it is composed mostly of hydrocarbon molecules which are too large to be soluble in common organic solvents.

In line with expectations, the powder collected after 18 h annealing of  $C_{60}$  at 550 °C had a weight loss of about 50% due to sublimation of reaction products. The samples obtained after hydrogen annealing at 500 and 550 °C were mostly not soluble. Therefore, we performed characterization of as-prepared powder and then extracted the soluble fraction for separate analysis (see next section).

Raman spectra recorded from powders obtained by hydrogen annealing at 500 and 550 °C are shown in Figure 1. It should be noted that fullerenes  $C_{60}H_x$  obtained in our previous studies using lower hydrogenation temperatures typically exhibited very strong luminescence background, and their Raman spectra could not be recorded with 514, 633, 780 nm lasers. Figure 1 shows that some luminescence background is still present in the spectra of 500 °C sample and completely disappeared in 550 °C sample indicating the absence of hydrogenated fullerenes in these samples. Figure 1 shows two broad features in the spectral region typical for G and D bands of amorphous carbon. However, unlike true amorphous carbon, the spectra exhibit several other peaks, while the G- and D-bandlike features clearly consist of several components. This type of spectrum is typical for larger PAHs molecules; see for example spectra of  $C_{78}$  and  $C_{114}$  in ref 23. Analysis of Raman spectra from various progressively larger PAHs was reported for example in a study by Castiglioni et al.<sup>24</sup> which demonstrated how spectral features

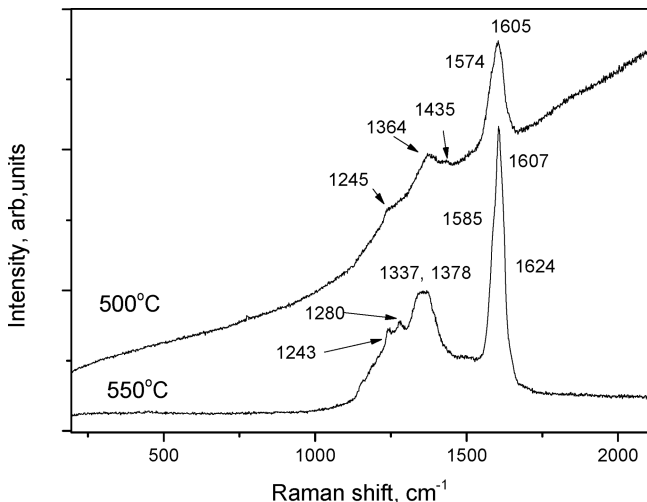


**Figure 1.** Raman spectra recorded from carbon deposits obtained by hydrogen annealing of  $C_{60}$  at 500 and 550  $^{\circ}\text{C}$ .

of “nano-graphenes” (see also ref 25) are transformed into G- and D-bands when the molecule size is increased.

More detailed information about composition of samples can be extracted from Fourier transform infrared (FTIR) spectra. Figure 2 shows spectra recorded from powders hydrogenated at 450  $^{\circ}\text{C}$  (mostly hydrogenated fragmented fullerenes and some PAHs<sup>12</sup>) and samples hydrogenated at 500 and 550  $^{\circ}\text{C}$ . Strong broadening of all spectral features and appearance of new ones are obvious for the samples hydrogen annealed at higher temperatures. Especially clear is the difference in the region of C–H vibrations ( $2700\text{--}3200\text{ cm}^{-1}$ ). In Figure 2, the arrow points at the major peak at  $3089\text{ cm}^{-1}$  with a smaller component at  $3083\text{ cm}^{-1}$ , see Table 1. The latter becomes progressively stronger when the temperature of hydrogen annealing is increased. The peaks are in the spectral region typical for C–H of PAH molecules and are assigned to large fragments of the  $C_{60}$  cage formed as a result of cage unzipping.

The spectral region  $2800\text{--}3000\text{ cm}^{-1}$  also shows a very complex combination of C–H peaks with several components distinguished (see Table 2S and deconvolution plots in Supporting Information); these peaks are distinctly different compared to peaks found in this region for highly hydrogenated  $C_{60}\text{H}_x$ . As noted above, formation of  $C_{60}\text{H}_x$  as a major product is not expected at 500–550  $^{\circ}\text{C}$  as these temperatures are above

**Table 1. Peak Positions (Region of C–H Vibrations)**  
Deconvoluted from Spectra Shown in Figure 2a

hydrogenated 450 $^{\circ}\text{C}$ 72 h (mostly $C_{60}\text{H}_x$ )	hydrogenated 550 $^{\circ}\text{C}$ 18 h
	2825
2843	2844
2872	2869
2895	2897
2926	2915
2959	2949
	3003
3038 (weak)	3039 (strongest)
	3083

the stability limit of C–H bonds in fullerenes. Therefore, most of the peaks observed in the FTIR spectra should be assigned to various (noncage) hydrocarbon molecules.

The collapse of the  $C_{60}$  cage structure is relatively rapid as confirmed by the FTIR spectra recorded from powder samples obtained by hydrogen annealing at 500  $^{\circ}\text{C}$  for 6 and 24 h, shown in Figure 2b. The spectra are almost identical, which demonstrates that reaction was mostly completed after 6 h. Raman and FTIR spectra prove that the samples obtained by hydrogen annealing do not consist anymore of fullerenes or their hydrogenated modifications. The spectra point to formation of larger hydrocarbon molecules.

However, the samples are even more complex as revealed by high resolution TEM images; see Figure 3. The analysis of TEM data shows that the sample prepared at 550  $^{\circ}\text{C}$  is mostly composed of few-layered (1–5 layers) defect graphene sheets. The FFT shows two circles of spots with  $d$ -spacings 2.27 and 1.26  $\text{\AA}$ , which correspond to graphene lattice while the distance between the layers is around 3.5  $\text{\AA}$ . The inset of Figure 3 shows a zoomed part of the sheet which exhibit some traces of periodicity, probably from the parent  $C_{60}$  lattice, as the size of spots which originate from corrugation of the 2D surface geometry corresponds approximately to the diameter of fullerene molecules. The graphene sheets can be formed as a result of hydrogen-driven  $C_{60}$  unzipping either by direct fusion of unzipped molecules or by reaction between  $C_{60}$  fragments formed as a result of cage collapse. The clues to understanding of the mechanism of hydrogen-driven  $C_{60}$  unzipping and fragmentation can be obtained by analysis of the soluble part of hydrogen-annealed samples; see next section.

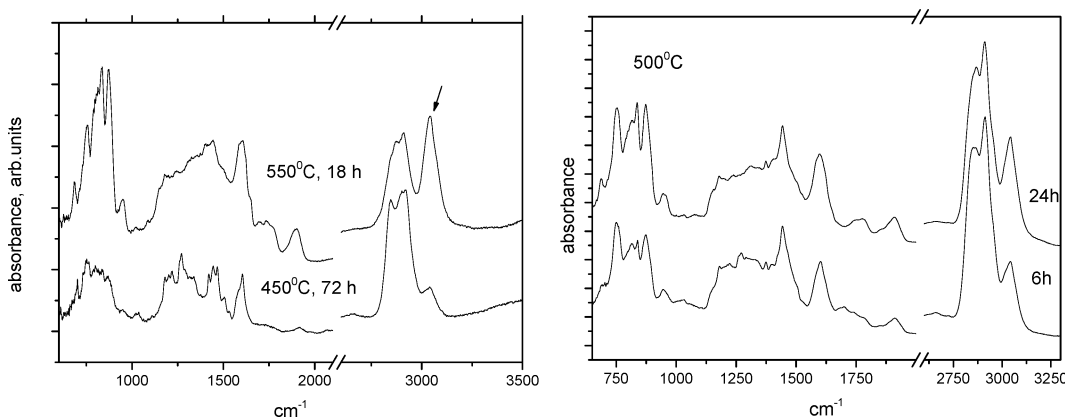


**Figure 2.** FTIR spectra recorded from (a) powder samples obtained by hydrogen annealing of  $C_{60}$  at 500 and 550  $^{\circ}\text{C}$ ; (b) powder samples obtained by hydrogen annealing at 500  $^{\circ}\text{C}$  with duration of treatment 6 and 24 h.

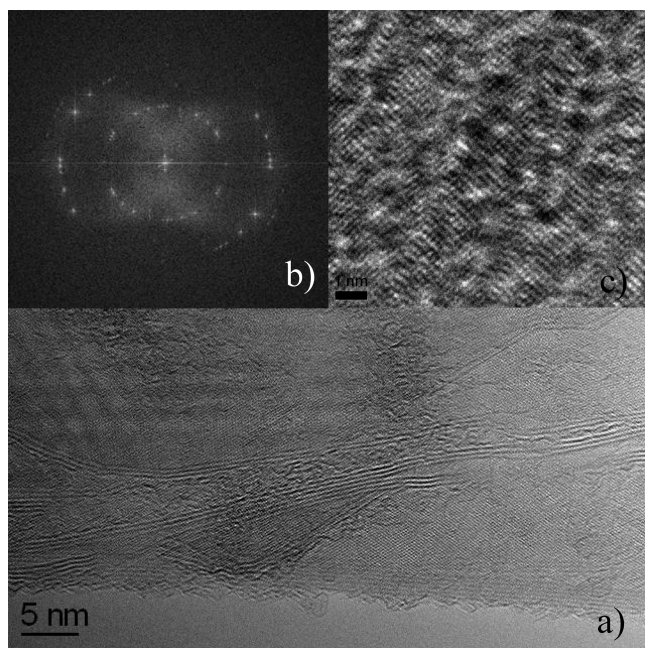


**Figure 3.** High resolution TEM recorded from the sample obtained by hydrogen annealing of  $C_{60}$  at 550 °C: (a) image showing defect few-layered graphene sheets, (b) FFT image, (c) zoomed area of graphene sheet.

**3.2. Analysis of the Soluble Part of Hydrogen Annealed Samples.** The solubility of samples produced from  $C_{60}$  by hydrogen annealing at 500 and 550 °C were tested for several common solvents, see Figure 4. The samples were subjected to sonication in toluene, acetone, dimethylformamide (DMF), and ethanol for a period of about 14 h. The best solubility was observed for DMF and toluene; no solubility was observed for ethanol. It is clear also that the sample prepared at lower temperature (500 °C) contains a larger fraction of



**Figure 4.** Solutions extracted from samples prepared by hydrogen annealing in visible and UV light. From the left to the right: DMF (500 and 550 °C samples), toluene (500 and 550 °C), acetone (500 and 550 °C), and ethanol (500 °C sample).

soluble products. Strong luminescence is typical for many PAH molecules; for example, perylene has very bright luminescence, whereas fullerene samples ( $C_{60}H_x$  with average composition  $x \sim 36$ ) do not show visible luminescence in UV light when dissolved in the same solvents. This further supports the assumption that fullerenes are not present in the samples of the present study.

The solutions were used for mass spectrometric characterization and NMR analysis. Using extraction with DMF and evaporation of solvent, we were able also to prepare several milligrams of powder which was used to record FTIR spectra, Figure 5. Comparing these spectra with spectra of parent powder allows one to distinguish contributions from soluble and nonsoluble fractions.

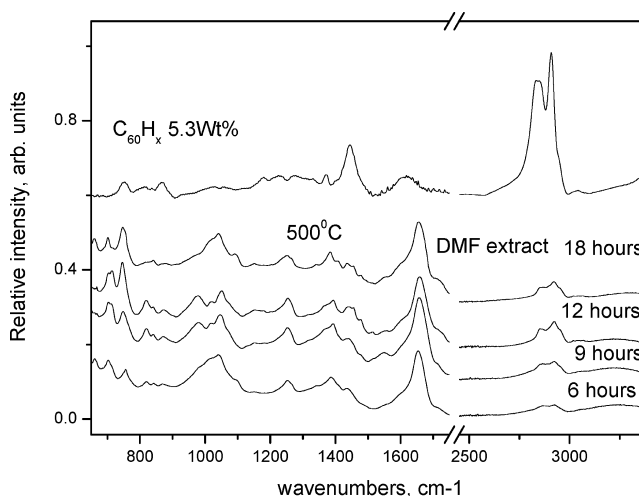


**Figure 5.** FTIR spectra recorded from DMF extracts prepared using  $C_{60}$  powder annealed in hydrogen at 500 °C with variation of treatment duration. The reference spectrum from mostly  $C_{60}H_x$  sample prepared at 450 °C is shown as a reference.<sup>12</sup>

The spectra shown in Figure 5 are clearly distinct from spectra of  $C_{60}H_x$  once again proving that no hydrogenated  $C_{60}$  is present in these samples. This difference is particularly clear in the region of C–H vibrations, where the strongly hydrogenated  $C_{60}$  sample (synthesized by reaction with  $H_2$  gas at 400 °C) showed four major peaks at 2826, 2858, 2909, and 2946  $\text{cm}^{-1}$ . The main peaks found in DMF extracts of the sample hydrogen annealed at 500 °C for 18 h are found at 2858, 2898, 2925, and 2955  $\text{cm}^{-1}$ ; see all peak positions found for these samples in Table 1S, Supporting Information. Figure 5 also shows that prolonging the duration of hydrogen annealing does not result in significant changes in composition of products: already after 6 h of treatment all fullerenes are transformed into hydrocarbons.

The relative intensity of C–H vibrations in DMF extracts is significantly lower compared to the spectrum obtained for fullerenes. This indicates a lower relative proportion of hydrogen atoms in these samples. Indeed, the fullerene sample shown in Figure 5 has at least two-thirds of carbon atoms hydrogenated (the maximal possible C/H ratio is 1:1 for  $C_{60}H_{60}$  fullerene), while for planar hydrocarbon molecules only carbon atoms situated on the edges of molecules are hydrogenated. Therefore, for larger planar PAH compounds, weaker C–H peaks can be expected than for smaller PAHs.

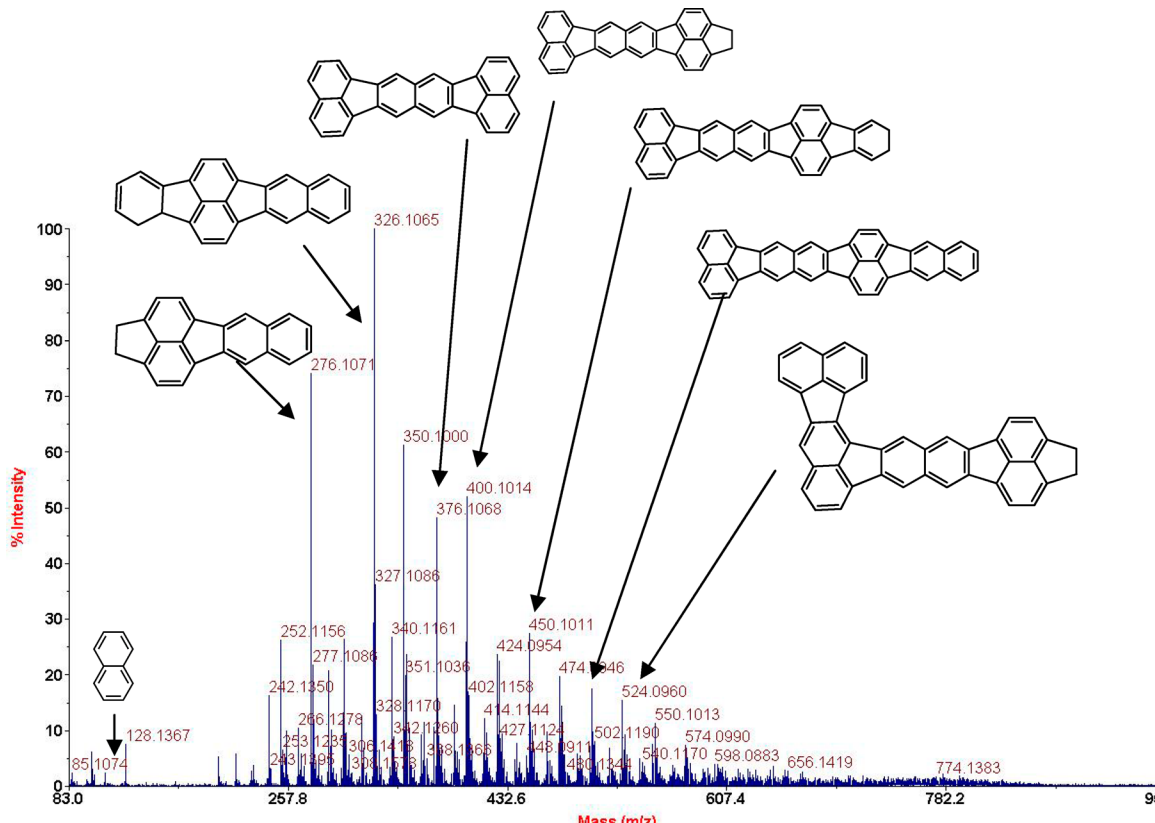


**Figure 6.** MALDI-MS spectrum of DMF extract from sample hydrogen annealed at 500 °C with hypothetical assignment of some major peaks.

It is also very interesting to compare the spectra of the DMF-extracted powders with those of the parent powder samples of Figure 2. The main difference is the absence of  $3039\text{ cm}^{-1}$  and  $3083\text{ cm}^{-1}$  peaks in the spectra of the extracted fraction. These peaks can be confidently assigned then to C–H vibrations of insoluble larger PAHs which are basically fragments of graphene sheets (“nanographenes”) terminated by hydrogen atoms.

This suggestion is also compatible with numerous peaks observed in the  $700\text{--}1000\text{ cm}^{-1}$  region of FTIR spectra. Considering the complex nature of samples composed of at least several main products, precise evaluation of the molecular composition using FTIR is not possible. However, one can note that several larger PAHs consisting of hexagons and pentagons (with geometry that corresponds to  $\text{C}_{60}$  cage fragments) are known to exhibit peaks in the this spectral region. For example, the FTIR spectrum of benzo[k]fluoranthene has major peaks at  $\sim 746\text{ cm}^{-1}$ ,  $823\text{ cm}^{-1}$ , and  $883\text{ cm}^{-1}$ , and the related benzo[j]fluoranthene has peaks at  $739\text{ cm}^{-1}$ ,  $769\text{ cm}^{-1}$ , and  $815\text{ cm}^{-1}$  assigned to out-of-plane CH bending vibrations typical for molecules containing aromatic or condensed aromatic rings. Spectra recorded from the hydrogen collapsed  $\text{C}_{60}$  samples showed peaks at similar positions,  $747\text{--}757\text{ cm}^{-1}$ ,  $820\text{--}823\text{ cm}^{-1}$ , and  $866\text{--}873\text{ cm}^{-1}$  (Table 2S, Supporting Information).<sup>26</sup>

Molecular compositions of DMF extracts were also studied using mass spectrometry. The mass spectrum recorded from the sample obtained by hydrogen annealing at 500 °C shows a very complex mixture of products with masses below  $\sim 600$  amu, Figure 6. The molecules lighter than 250 amu are almost absent in the spectrum, which is the expected result: light hydrocarbons with low melting points evaporate from the

powder samples in the process of hydrogen annealing. Remarkably, this spectrum shows no peaks from pristine  $\text{C}_{60}$  (720 amu) or hydrogenated fragmented fullerenes which are typically found in the samples hydrogenated at lower temperatures (400–450 °C) after prolonged reaction durations.<sup>12,14</sup>

The spectrum shown in Figure 6 exhibits a very distinct pattern with strongest peaks in the following trend: peaks with  $\text{C}_2$  (24 amu) difference and with  $\text{C}_2\text{H}_2$  difference (26 amu). These peaks are interpreted as chain products of  $\text{C}_{60}$  cage fragmentation with a consequently smaller size of fragments. It should be emphasized that the peaks observed in this spectrum represent true composition of products present in our sample and cannot be assigned to fragmentation of larger molecules induced in the process of MS recording. This conclusion is supported by a separate experiment where we attempted to separate reaction products obtained by hydrogen annealing of  $\text{C}_{60}$  using sublimation with a temperature gradient inside of vacuum sealed glass tube. As a result of this experiment, we observed differently colored areas in the reaction tube with orange products accumulated in the region of higher temperatures, yellowish products in the colder part, and some microcrystals precipitated in the coldest part of the tube. The microcrystals were unambiguously identified using Raman spectroscopy as pyrene, while yellow and orange fractions of the samples exhibited luminescence background, which do not allow recording of Raman spectra. MALDI-MS from orange and yellow sublimation products indeed showed that they consist of heavier and lighter molecular species (see Figure 2S in Supporting Information) with major MS peaks corresponding to the overall composition of parent sample which was similar to the spectrum shown in Figure 6. This experiment

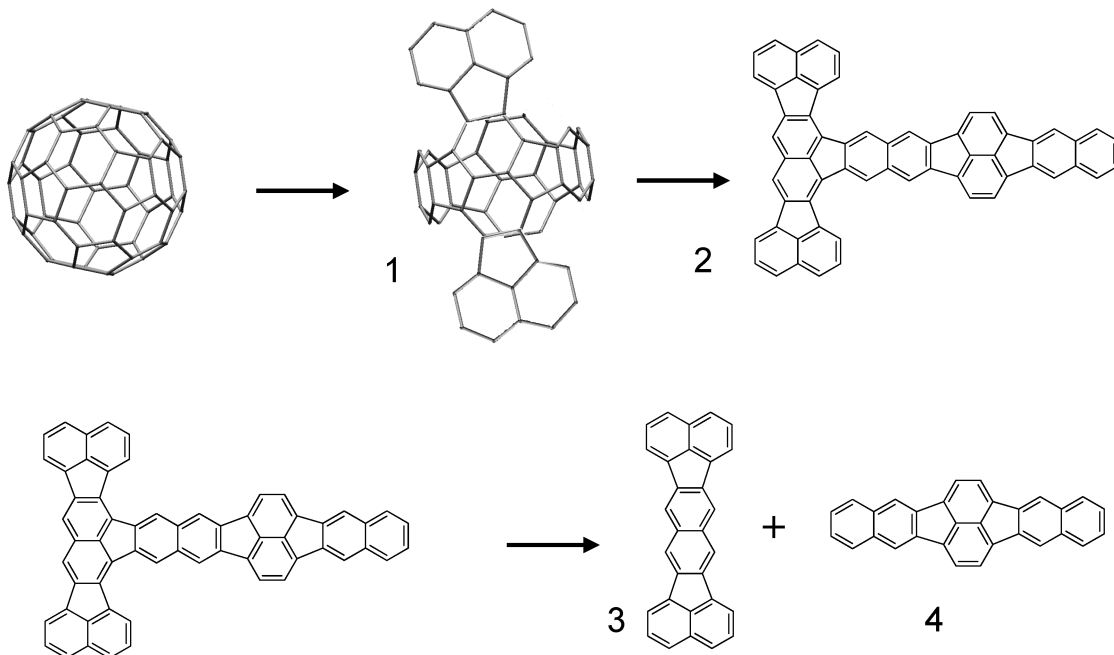


**Figure 7.** Suggested model of  $C_{60}$  fragmentation driven by reaction with hydrogen.

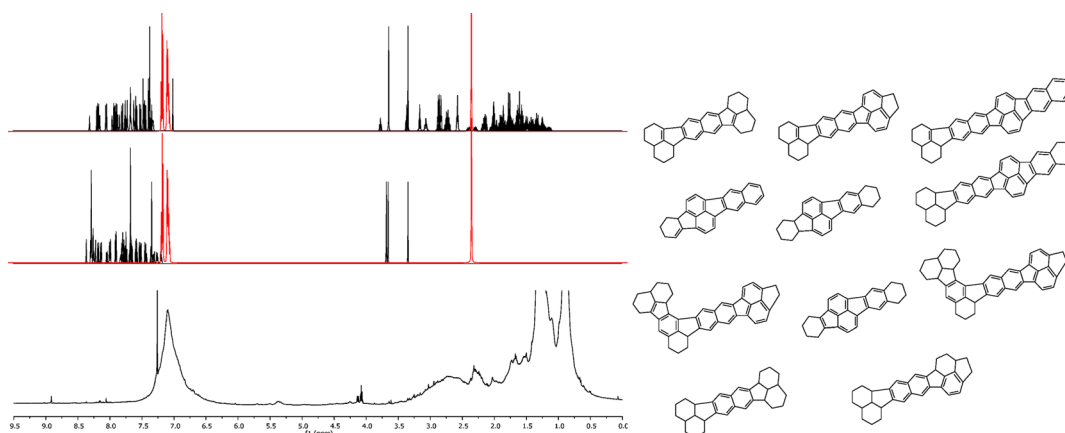


**Figure 8.** Lower trace, left panel:  $^1\text{H}$  NMR in toluene- $d_8$  of toluene-soluble fraction of “Batch 2”, produced at 550 °C. Middle trace: Simulated chemical shifts for the PAH structures suggested from the MALDI-MS data. Upper trace: Simulated chemical shifts for partly reduced PAHs (depicted in panel right). Simulated signals in red are for toluene (extraction solvent for “Batch 2” and likely the most soluble arene component of the sample).

proves that major peaks observed in the mass spectra of our samples can be considered mostly as true fragments of the  $C_{60}$  cage, not a result of fragmentation induced in the process of MS recording. It is impossible to identify all peaks observed in Figure 6 with certain molecules, but analysis of trends allows one to make reasonable suggestions about possible fragmentation path of the  $C_{60}$  cage in the hydrogen driven collapse process.

It is logical to suggest that most abundant products of  $C_{60}$  fragmentation and collapse will consist only of pentagons and hexagons; these molecules should also be molecular fragments of the fullerene cage terminated by hydrogen atoms. Below we propose a possible model of  $C_{60}$  fragmentation which is speculated to explain the sequence of peaks found in the MS spectra (see Figure 7). The model suggests direct unzipping of the  $C_{60}$  molecule with formation of mostly flat molecules. The cuplike molecules (e.g., corannulene) are less likely to appear as major products due to their lower stability caused by strain.

The molecule 2 represents flat hydrocarbon consisting of 60 carbon atoms which can be obtained from  $C_{60}$  by consequent breaking of some C–C bonds on pentagon–hexagon edges. One of the possible intermediate products which illustrate a pathway of unzipping is shown in Figure 7 as molecule 1. Most of the peaks observed in the mass spectra of our samples now can be explained if we suggest that they are formed by the breakup of molecule 2 on smaller fragments which consist of pentagons and hexagons; one example of such fragmentation is shown in Figure 7 and results in formation of molecules 3 and 4. Figure 6 shows possible assignment of peaks found in our spectra using various fragments of molecule 2 produced by cage unzipping of  $C_{60}$ . Of course, more than one fragmentation pathway is possible in the process of hydrogen driven fragmentation of  $C_{60}$ .

Detailed analysis of the hydrocarbon species present in solvent extracted samples (e.g., using separation by HPLC) was so far not successful due to the very complex sample

compositions and, for chromatography purposes, poor solubility. However, some of evidence supporting the suggested fragmentation model was obtained using NMR analysis of soluble reaction products from two reaction temperatures; the parent powder of batch 1 was produced at 500 °C and that of batch 2 at 550 °C.

The  $^1\text{H}$  NMR analysis indicates the presence of aromatic and polycyclic structure elements as well as branched and nonbranched aliphatic hydrocarbons, some of which may be attached to aromatic units (Figure 8, lowest trace). In both batches, the more prominent signals are from residual extraction solvent (mainly toluene). The relative proportion of vinylic/alkynic hydrogens in conjugated alkene–alkene/alkyne or arene–alkene/alkyne structural elements (5–7 ppm) is lower than the relative proportion of hydrogens in arene (6–8 ppm) and aliphatic (0–4 ppm) structural elements. The relative proportion of aromatic structures is lower in batch 2 than in batch 1, and the observed chemical shifts are quite consistent with what should be expected from a mixture of the compounds detected in the MALDI-MS analyses (simulated, middle trace of Figure 8). The broad signals in the aliphatic region indicate the presence of compounds even further reduced. Assuming hydrogenation at the more reactive positions of the set of compounds used for the generation of the middle trace, the chemical shift simulation of the mixture gives a spectrum even closer to the experimental ones, considering only the chemical shifts as the simulations were carried out for unlikely mixtures with one entity of each compound and toluene. The further reduced compounds, having  $\text{sp}^3$  centers, should be more soluble in used solvents than the more planar  $\text{sp}^2$  PAH degradation products, and hence the relative proportion detected by  $^1\text{H}$  NMR is not reflecting the composition of the entire sample. Moreover, it is not unlikely that certain unsaturated degradation products undergo oligomerization or rearrangement processes, leading to even more complex mixtures. The signals at 8–9 ppm are indicative of aldehyde groups. Such functional groups may form by oxidation of terminal allylic or certain benzylic positions in air. Both oligomerization and partial aerobic oxidations are likely during the sonication-assisted extraction and subsequent solvent evaporation, and would explain the (poor) solubility and macroscopic “sticky” appearance of the materials.

The presence of aliphatic structural elements is evident also from the  $^{13}\text{C}$  NMR spectrum of batch 2 (not shown), with four signals in the region 10–35 ppm. Arene signals from the sample, except for the signal originating from the very small quantity of unreacted  $\text{C}_{60}$  (hardly distinguishable on TLC) are expected to be buried in the solvent signal. Summarizing the NMR data, aromatic and polycyclic structural elements are present in studied samples, and the sample annealed in hydrogen at higher temperature shows larger proportion of these elements as expected in fragmentation pathway shown in Figures 6 and 7.

In conclusion of this section, the soluble fraction of hydrogen-collapsed  $\text{C}_{60}$  samples represents smaller part of the as-produced powders but allows the proposal of a pathway for the fragmentation of fullerene into PAH entities with carbon skeletons that correspond to fragments of the cage structure. More detailed analysis of the mixture of molecules is complicated not only by complex combinations of such fragments in the studied samples but also by reaction of these fragments with each other. The larger part of our samples consist of nonsoluble molecules and few-layered graphene

sheets revealed in our samples, which points to reactions that include fusion of the planar  $\text{C}_{60}$  fragments into nanographenes of progressively larger size.

**3.3. Hydrogen Annealing of  $\text{C}_{60}$  Thin Films: Formation of Graphene Islands.** The few-layered graphene sheets found in powder samples of hydrogen-collapsed  $\text{C}_{60}$  indicated a hypothetical possibility to synthesize single-layered graphene using  $\text{C}_{60}$  as a precursor. We suggested that using sufficiently thin film of  $\text{C}_{60}$  for hydrogen annealing reaction may result in surface-assisted formation of single-layered graphene instead of few-layered sheets randomly formed in the powder. To test the hypothesis,  $\text{C}_{60}$  films of different thickness were deposited on gold-plated mica substrates and subjected to hydrogen annealing at 550 °C at the conditions similar to those used for powders. A significant part of the material was expected to evaporate from the initial films in the form of gaseous hydrocarbons, similar to experiments with bulk powders described above. Analysis of the films after hydrogen treatment revealed that at least part of carbon material formed because hydrogen-driven fullerene fragmentation had preserved as thin film on the gold surface.

The Raman spectra recorded from the films revealed a significant difference compared to the spectra collected from bulk powders, and the difference is especially strong for the thinnest films; see Figure 9. The film with an initial thickness of

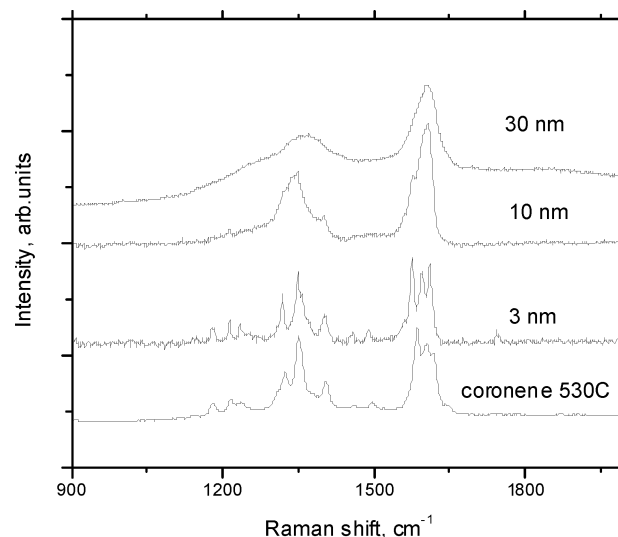


**Figure 9.** Raman spectra recorded from  $\text{C}_{60}$  films of various initial thicknesses subjected to hydrogen annealing at 550 °C.

30 nm showed Raman spectra similar to those of bulk powder samples: only two broad but rather asymmetric features which correspond to multicomponent D- and G-bands of larger PAHs or defected graphitic carbon. The peaks become less broad in the spectra recorded from film with an initial thickness of 10 nm, with some clearly distinct peaks that indicate a larger fraction of nanographenes and hydrocarbon molecules.

The thinnest  $\text{C}_{60}$  films (initial thickness of 3 nm) consisted of only 4–5 monolayers of  $\text{C}_{60}$  molecules prior the reaction. Raman spectra recorded from this film after hydrogen annealing showed strikingly different features with a number of rather sharp peaks. It should be noted that many accumulations had to be used to collect the spectra due to small thickness of resulting films and weak signals. The spectra exhibit three distinct and rather sharp peaks instead of a broad

G-band feature, whereas D-band region exhibits several peaks spread over a broader spectral range. The sharp peaks found in the spectra are indicative of a more homogeneous reaction product formed in the thinnest films. According to the data obtained for bulk powders, it is expected also that at least one-half of the material is evaporated from the films in the form of gaseous hydrocarbons.

The Raman spectra recorded from thinnest hydrogen annealed films show striking similarity to the previously reported Raman spectra of coronene annealing products (coronene oligomers). The spectrum recorded from bulk toluene-insoluble sample produced by heat treatment of coronene is shown as a reference in Figure 9.<sup>20</sup> The detailed molecular structure of coronene oligomers is not completely clear, but likely they consist of linear or possibly branched coronene chains of various length. Observation of similar spectral features in hydrogen-collapsed  $C_{60}$  samples was completely unexpected. Therefore, we repeated the same set of experiments, again using three  $C_{60}$  films with different thicknesses to verify reproducibility of the thickness-dependent effect in the hydrogen annealing treatment.

The second set of experiments showed the same trends: very broad spectral features were observed for films with higher thickness and many sharp peaks for thinnest films. The peak positions found for thinnest films almost exactly coincide with the spectra of coronene oligomers.<sup>20</sup> Coronene and diconylenes (coronene dimer) would sublime away from our samples at the temperature of reaction, and only larger molecules could survive annealing and preserve on the substrate. Therefore, the Raman peaks are likely to originate from larger nanographenes formed by fusion of coronene-like PAH molecules formed on the substrate at 550 °C. It is interesting that coronene is not a fragment of the  $C_{60}$  cage structure as it consists of six hexagons fused into a ring. Therefore, the coronene oligomers cannot be formed only as a result of  $C_{60}$  unzipping and most likely formed in surface-assisted reactions between fullerene fragments. This suggestion is confirmed by observation of spectral features from coronene oligomers only in the thinnest of hydrogen-annealed  $C_{60}$  films.

The collapse of  $C_{60}$  molecules in thin films subjected to hydrogen annealing at 550 °C was confirmed also using XPS. The films were characterized by XPS before and after hydrogen treatment. The spectrum of a pristine 1–3 nm thick film was typical for  $C_{60}$  spectrum with the C1s peak at 284.5 eV. The film was not continuous as evident from detection of 29.9 atom % of gold (from material of substrate). The proportion of gold increased after hydrogen annealing of the film to 55.5 atom %. That is in good correlation with experiments on powder samples described above where about 50% mass loss was observed as a result of the hydrogen treatment. The new nanographene carbon phase is characterized by a shift of the main C1s peak to 284.3 eV and new weaker peaks found at 285.7 eV (due to C–H) and 287.1 eV, which is possibly a result of partial sample oxidation after exposure to air (see Supporting Information).

The characterization of nanographene islands was performed also using AFM and STM, and the conductivity of individual islands was measured.

**3.4. AFM, STM, and Conductivity.** The characterization of hydrogen-annealed films was performed using AFM and STM, and conductivity of individual islands was measured. Figure 10 shows AFM and STM topographic images of islands formed by hydrogen annealing of thinner  $C_{60}$  film deposited on

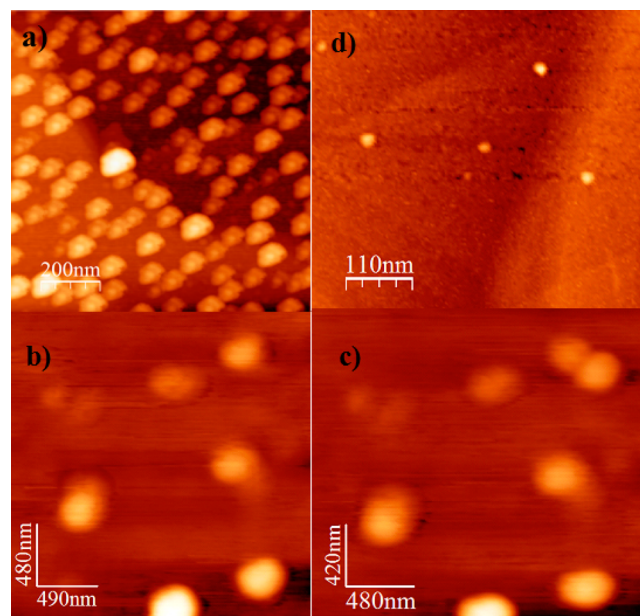


**Figure 10.** Topographic AFM images in tapping mode: (a) nanoislands formed by hydrogen collapse of  $C_{60}$  thin film (b) individual nanoislands before exfoliation (c) after exfoliation; (d) STM image of island on the Au(111) surface. Scanning parameter are 0.5 nA and 0.6 V for tunneling current and sample bias respectively.

the gold surface. The islands are homogeneous in size and uniformly cover the entire scan area. The average size of islands is 50 nm and height is about 10 nm. We selected several islands to perform local electrical conductivity measurements at 15 spots on each island, Figure 11. An Ohmic behavior at low bias

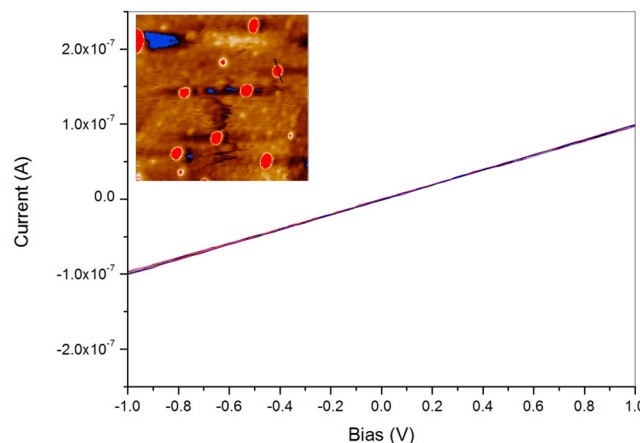


**Figure 11.** Local voltage-current graph measured on nanoisland (shown in the inset). The curves exhibit linear behavior, indicating the metallic character for the nanoislands. To protect the island and the AFM tip from atom migration, the maximum current was set to 0.1 microamp using a series resistor of 10 MΩ.

was observed with no saturation at higher voltages indicating a metallic behavior that is completely different from the pristine parent  $C_{60}$  material which is known to be a semiconductor.

Moreover, the island can be exfoliated using an AFM tip at a relatively low lateral force of 100  $\mu$ N as shown in Figure 10b,c, indicating weak vertical bonding and evidence of multilayered structures. In this experiment, the tip is moved laterally about 50 nm away from the edge of a designated nanoisland, and then

the feedback loop is interrupted and the tip is brought 5–10 nm above the gold surface. As scanning is resumed (without feedback control), the tip suffers a torque due to shear stress as it reaches the island about 5–10 nm below its surface. This torque causes the AFM tip to exert a horizontal force as it scans through the island. Bond rupturing occurs when this force is larger than bonding forces and finally exfoliating the nanoisland. We find also that the island formed by exfoliation maintained its metallic characters similar to its parent island.

The change in electrical character of  $C_{60}$  materials after the hydrogenation process has prompted us to conduct STM measurements as shown in Figure 10d. Unlike the case of pure  $C_{60}$  islands of similar height, which could not be imaged with STM, the imaging of transformed materials can be established at low bias of 0.2 V and tunneling current of 0.1 nA. The average size of the islands is about 30 nm with a height of 15 nm.

Therefore, it can be concluded that thin  $C_{60}$  films exposed to hydrogen treatment at 550 °C have been transformed into few-layered nanographene islands. The AFM/STM results are also in agreement with Raman spectra recorded from thin films which are typical for large hydrogen-terminated nanographene samples.<sup>20</sup>

The experiments performed here could serve as a proof of concept for the possibility to prepare graphene films by hydrogen annealing of thin fullerene film. Simple calculation shows that the number of carbon atoms in a monolayer  $C_{60}$  film is sufficient only for the formation of double-layered graphene film. Considering that some carbons are evaporated in the process of hydrogen annealing in form of light gaseous hydrocarbons, it is reasonable to suggest that the synthesis of single-layered graphene might be possible in the future using a  $C_{60}$  precursor and hydrogen annealing. The advantage of such a synthesis method would be the low temperatures required for  $C_{60}$  film deposition, the variety of possible substrates available, and the homogeneous hydrogen termination of graphene edges.

#### 4. CONCLUSIONS

Hydrogen annealing of bulk  $C_{60}$  powders and thin films at elevated conditions (above the temperature of C–H bond stability in  $C_{60}H_x$ ) results in the collapse of the  $C_{60}$  cage structure. Analysis of reaction products includes both the soluble and the insoluble parts. The insoluble fraction is composed of nanographenes and few-layered graphene sheets, whereas the soluble part of the hydrogen-collapsed  $C_{60}$  samples is a complex mixture of hydrocarbon molecules, which represent fullerene cage fragments of different sizes. Considering higher relative abundance of peaks with a mass difference corresponding to  $C_2H_2$ , we suggest a possible pathway for  $C_{60}$  cage unzipping followed by breakup with formation of planar PAH fragments with a progressively smaller size. The pathway allows assigning most of the peaks in the complex mass spectrum of the hydrogen collapsed sample to a sequence of planar polycyclic aromatic molecules formed by carbon pentagons and hexagons. Prolonged hydrogen annealing is likely to result also in fusion of fullerene cage fragments into few-layered defect graphene sheets.

Hydrogen annealing of  $C_{60}$  thin films at the conditions of cage collapse and fragmentation resulted in formation of nanographene islands which exhibited Raman spectra with surprising similarity to products of coronene annealing (coronene oligomers).

The conductivity tests performed on single nanoislands showed IV dependence typical for graphene. Therefore, it can be suggested that hydrogen annealing of thin  $C_{60}$  films can be used in the future for synthesis of few-layered and single-layered hydrogen-terminated graphene samples.

#### ■ ASSOCIATED CONTENT

##### S Supporting Information

Deconvolution plots for FTIR spectra; full table with FTIR peak positions; MALDI-TOF spectra recorded for precipitate deposited in colder and hotter zones after sublimation of “collapsed  $C_{60}$ ” sample with temperature gradient; Raman spectra recorded from second set of hydrogen-collapsed  $C_{60}$  films (similar to experiments shown in Figure 9S). This information is available free of charge via the Internet at <http://pubs.acs.org>

#### ■ AUTHOR INFORMATION

##### Corresponding Author

\*E-mail: [Alexandr.talyzin@physics.umu.se](mailto:Alexandr.talyzin@physics.umu.se).

##### Notes

The authors declare no competing financial interest.

#### ■ ACKNOWLEDGMENTS

This work made use of the Aalto University Nanomicroscopy Center (Aalto-NMC) premises. We thank A. Schinkarev for help with XPS. This work was financially supported (A.T.) by the Swedish Research Council, Grant No. 621-2012-3654 and (H.G.) the Uppsala University KoF07 program for graphene, the Knut and Alice Wallenberg foundation, and the Swedish Research Council, grant No. 621-2010-7499.

#### ■ REFERENCES

- (1) Attalla, M. I.; Vassallo, A. M.; Tattam, B. N.; Hanna, J. V. Preparation of Hydrofullerenes by Hydrogen Radical-Induced Hydrogenation. *J. Phys. Chem.* **1993**, *97*, 6329–6331.
- (2) Jin, C. M.; Hettich, R.; Compton, R.; Joyce, D.; Blencoe, J.; Burch, T. Direct Solid-Phase Hydrogenation of Fullerenes. *J. Phys. Chem.* **1994**, *98*, 4215–4217.
- (3) Darwish, A. D.; Avent, A. G.; Taylor, R.; Walton, D. R. M. Structural Characterisation of  $C_{60}H_{18}$ ; a C-3v Symmetry Crown. *J. Chem. Soc., Perkin Trans. 2* **1996**, 2051–2054.
- (4) Loufty, R. O.; Wexler, E. M. In *Perspectives of Fullerene Nanotechnology*; Springer, Netherlands, 2002; pp 281–287.
- (5) Shul'ga, Y. M.; Tarasov, B. P.; Fokin, V. N.; Martynenko, V. M.; Schur, D. V.; Volkov, G. A.; Rubtsov, V. I.; Krasochka, G. A.; Chapusheva, N. V.; Shevchenko, V. V. Deuterofullerenes. *Carbon* **2003**, *41*, 1365–1368.
- (6) Elias, D. C.; Nair, R. R.; Mohiuddin, T. M. G.; Morozov, S. V.; Blake, P.; Halsall, M. P.; Ferrari, A. C.; Boukhvalov, D. W.; Katsnelson, M. I.; Geim, A. K.; et al. Control of Graphene's Properties by Reversible Hydrogenation: Evidence for Graphane. *Science* **2009**, *323*, 610–613.
- (7) Teprovich, J. A.; Wellons, M. S.; Lascola, R.; Hwang, S. J.; Ward, P. A.; Compton, R. N.; Zidan, R. Synthesis and Characterization of a Lithium-Doped Fullerene ( $Li_xC_{60}H_y$ ) for Reversible Hydrogen Storage. *Nano Lett.* **2012**, *12*, 582–589.
- (8) Mauron, P.; Remhof, A.; Bliersbach, A.; Borgschulte, A.; Zuttel, A.; Sheptyakov, D.; Gaboardi, M.; Choucair, M.; Pontiroli, D.; Aramini, M.; et al. Reversible Hydrogen Absorption in Sodium Intercalated Fullerenes. *Int. J. Hydrogen Energy* **2012**, *37*, 14307–14314.
- (9) Talyzin, A. V.; Sundqvist, B.; Shulga, Y. M.; Peera, A. A.; Imus, P.; Billups, W. E. Gentle Fragmentation of  $C_{60}$  by Strong Hydro-

- genation: a Route to Synthesizing New Materials. *Chem. Phys. Lett.* **2004**, *400*, 112–116.
- (10) Talyzin, A. V.; Shulga, Y. M.; Jacob, A. Comparative Study of Hydrofullerides C<sub>60</sub>H<sub>x</sub> Synthesized by Direct and Catalytic Hydrogenation. *Appl. Phys. A* **2004**, *78*, 1005–1010.
- (11) Talyzin, A. V.; Tsybin, Y. O.; Peera, A. A.; Schaub, T. M.; Marshall, A. G.; Sundqvist, B.; Mauron, P.; Zuttel, A.; Billups, W. E. Synthesis of C<sub>59</sub>H<sub>x</sub> and C<sub>58</sub>H<sub>x</sub> Fullerenes Stabilized by Hydrogen. *J. Phys. Chem. B* **2005**, *109*, S403–S405.
- (12) Talyzin, A. V.; Tsybin, Y. O.; Purcell, J. M.; Schaub, T. M.; Shulga, Y. M.; Noreus, D.; Sato, T.; Dzwilewski, A.; Sundqvist, B.; Marshall, A. G. Reaction of Hydrogen Gas with C-60 at Elevated Pressure and Temperature: Hydrogenation and Cage Fragmentation. *J. Phys. Chem. A* **2006**, *110*, 8528–8534.
- (13) Talyzin, A. V. Fullerenes by Direct Reaction with Hydrogen Gas at Elevated Conditions. *Carbon Mater.: Chem. Phys.* **2010**, *2*, 85–103.
- (14) Luzan, S. M.; Tsybin, Y. O.; Talyzin, A. V. Reaction of C<sub>60</sub> with Hydrogen Gas: In Situ Monitoring and Pathways. *J. Phys. Chem. C* **2011**, *115*, 11484–11492.
- (15) Schur, D. V.; Zaginaichenko, S. Y.; Savenko, A. F.; Bogolepov, V. A.; Anikina, N. S.; Zolotarenko, A. D.; Matysina, Z. A.; Veziroglu, T. N.; Skryabina, N. E. Experimental Evaluation of Total Hydrogen Capacity for Fullerite C-60. *Int. J. Hydrogen Energy* **2011**, *36*, 1143–1151.
- (16) Luzan, S. M.; Cataldo, F.; Tsybin, Y. O.; Talyzin, A. V. Thermal Decomposition of C<sub>60</sub>H<sub>18</sub>. *J. Phys. Chem. C* **2009**, *113*, 13133–13138.
- (17) Cataldo, F. Fullerane, the Hydrogenated C(60) Fullerene: Properties and Astrochemical Considerations. *Fullerenes, Nanotubes, Carbon Nanostruct.* **2003**, *11*, 295–316.
- (18) Cataldo, F.; Iglesias-Groth, S. Characterization of Hydrogenated Fullerene Mixture of C<sub>60</sub>H<sub>x</sub> and C<sub>70</sub>H<sub>x</sub>. *Fullerenes, Nanotubes, Carbon Nanostruct.* **2010**, *18*, 97–106.
- (19) Talyzin, A. V.; Luzan, S. M.; Anoshkin, I. V.; Nasibulin, A. G.; Jiang, H.; Kauppinen, E. I. Hydrogen-Driven Collapse of C<sub>60</sub> Inside Single-Walled Carbon Nanotubes. *Angew. Chem., Int. Ed.* **2012**, *51*, 4435–4439.
- (20) Talyzin, A. V.; Luzan, S. M.; Leifer, K.; Akhtar, S.; Fetzer, J.; Cataldo, F.; Tsybin, Y. O.; Tai, C. W.; Dzwilewski, A.; Moons, E. Coronene Fusion by Heat Treatment: Road to Nanographenes. *J. Phys. Chem. C* **2011**, *115*, 13207–13214.
- (21) Talyzin, A. V.; Anoshkin, I. V.; Krasheninnikov, A. V.; Nieminen, R. M.; Nasibulin, A. G.; Jiang, H.; Kauppinen, E. I. Synthesis of Graphene Nanoribbons Encapsulated in Single-Walled Carbon Nanotubes. *Nano Lett.* **2011**, *11*, 4352–4356.
- (22) Kovac, A.; Znidarsic, A.; Jesih, A.; Mrzel, A.; Gaberscek, M.; Hassanien, A. A Novel Facile Synthesis and Characterization of Molybdenum Nanowires. *Nanoscale Res. Lett.* **2012**, *7*, 567–573.
- (23) Di Donato, E.; Tommasini, M.; Fustella, G.; Brambilla, L.; Castiglioni, C.; Zerbi, G.; Simpson, C. D.; Mullen, K.; Negri, F. Wavelength-Dependent Raman Activity of D-2h Symmetry Polycyclic Aromatic Hydrocarbons in the D-band and Acoustic Phonon Regions. *Chem. Phys.* **2004**, *301*, 81–93.
- (24) Castiglioni, C.; Mapelli, C.; Negri, F.; Zerbi, G. Origin of the D Line in the Raman Spectrum of Graphite: A Study Based on Raman Frequencies and Intensities of Polycyclic Aromatic Hydrocarbon Molecules. *J. Chem. Phys.* **2001**, *114*, 963–974.
- (25) Tommasini, M.; Castiglioni, C.; Zerbi, G. Raman scattering of molecular graphenes. *Phys. Chem. Chem. Phys.* **2009**, *11*, 10185–10194.
- (26) Hudgins, D. M.; Sandford, S. A. Infrared Spectroscopy of Matrix Isolated Polycyclic Aromatic Hydrocarbons. 3. Fluoranthene and the Benzofluoranthenes. *J. Phys. Chem. A* **1998**, *102*, 353–360.